Richtmyer-Meshkov Instability of a Membraneless, Sinusoidal Gas Interface

B.J. Motl, J.H.J. Niederhaus, M.H. Anderson, J.G. Oakley, R. Bonazza

July 2005

UWFDM-1300

Presented at the 25th International Symposium on Shock Waves (ISSW25), Bangalore, India, 17-22 July 2005.

FUSION TECHNOLOGY INSTITUTE

UNIVERSITY OF WISCONSIN

MADISON WISCONSIN

Richtmyer-Meshkov Instability of a Membraneless, Sinusoidal Gas Interface

B.J. Motl, J.H.J. Niederhaus, M.H. Anderson, J.G. Oakley, R. Bonazza

Fusion Technology Institute
University of Wisconsin
1500 Engineering Drive
Madison, WI 53706

http://fti.neep.wisc.edu

July 2005

UWFDM-1300

Presented at the 25th International Symposium on Shock Waves (ISSW25), Bangalore, India, 17-22 July 2005.

Richtmyer-Meshkov Instability of a Membraneless, Sinusoidal Gas Interface

B.J. Motl, J.H.J Niederhaus, M.H. Anderson, J.G. Oakley, and R. Bonazza

Department of Engineering Physics, University of Wisconsin-Madison, Madison, WI, USA

Abstract. A flat interface was created in a vertical shock tube by injecting a light gas from above, and a heavy gas from below, and then removing gas at the interface using a vacuum system. Once the flat stable interface was created, opposing rectangular pistons located in the walls of the interface section and spanning the width of the shock tube were oscillated to impose a sinusoidal perturbation on the interface. The light gas was seeded with acetone in order to utilize the planar laser-induced fluorescence (PLIF) imaging technique. The Richtmyer-Meshkov instability was then studied for an incident shock strength of M=1.3. Experimental images and time sequenced growth rates are compared to numerical simulations using the RAPTOR code (LLNL). RAPTOR takes advantage of the Piecewise Linear Method (PLM) with Adaptive Mesh Refinement (AMR) to solve the Navier-Stokes equations.

1 Introduction

The Richtmyer-Meshkov (RM) instability is a hydrodynamic instability that results from the misalignment of density and pressure gradients across a gas interface due to an impulsive force. The RM instability plays an important role in the field of inertial confinement fusion (ICF) because it is responsible for lowering the ICF energy yield by creating unwanted mixing of the pellet shell with the pellet fuel [1]. The RM instability also plays a role in supernova expansion [2] and supersonic mixing (as in a ramjet or scramjet engine).

Many different methods have been employed to study the RM instability in a shock tube. The first experiments were preformed by Ye. Ye. Meshkov, who used a thin nitrocellulose film (with a perturbation) to separate the test gases [3]. The film and the wires that support the film could distort the fluid flow and possibly weaken the transmitted shock wave. Oakley [4] utilized a technique that created a sinusoidal interface with a formed thin metal plate that was inserted into the shock tube. The plate was retracted before the shock wave traversed the interface; however, the initial conditions in this case can be non-linear and multi-valued due to vortex shedding off of the plate [5]. Recently, a new technique for creating an interface was developed by Jones and Jacobs [6]. This gas interface was created without any intrusive instruments (films, wire, plates) by introducing gas from opposite ends of the shock tube and then exiting through slots in the test section walls, which created a flat interface. The interface was then given a sinusoidal perturbation by oscillating the entire shock tube.

2 Experiment

The Wisconsin Shock Tube was used for the present experiments. The shock tube is vertical, downward firing, and has a total length of 9.2 m. The driver section is circular with a radius of 41 cm, while the driven section has an inner square cross section with 25 cm sides [7]. A high-pressure boost tank was connected to the driver section by a

pneumatically-driven fast-opening valve to control the diaphragm rupture time. The diaphragm used in these experiments was a 0.41 mm thick sheet of Al-3003 resulting in an incident shock strength of M=1.3. Piezoelectric pressure transducers were used to trigger the controlling electronics and to measure the shock speed.

The interface preparation method designed and used for this experiment is similar to the one used by Jones and Jacobs [6]. The interface section of the shock tube, shown in Fig. 1, was designed to accommodate two rectangular 5.08×25 cm aluminum pistons. The pistons have slots that were connected to a vacuum pump that was set to an outflow rate of 40.0 lpm. Sulfur-hexafluoride was introduced into the bottom of the shock tube at a flow rate of 9.3 lpm and nitrogen seeded with acetone was introduced into the shock tube just below the diaphragm at a rate of 30.8 lpm. The differences in flow rates account for different shock tube volumes above and below the interface. Acetone seeding was performed by running nitrogen through two consecutive acetone baths that were kept at a constant temperature of -4°C. On average, the mole fraction of acetone in the nitrogen/acetone mixture was 0.11. The pre-shock Atwood number for this gas is 0.65. The gases were continuously flown for 45 minutes at which point a repeatable flat interface was achieved. To generate a 2-D perturbation on the interface, the pistons were then driven by a stepper motor at a frequency of either 1.9 Hz (for 3 revolutions) or 2.6 Hz (for 4 revolutions), depending on the desired initial condition with a total piston travel of 2.86 cm. During the piston motion, electronic triggers were sent out to open the camera shutters, close the vacuum pump valve, and open the boost tank. A pressure transducer 0.71 m above the interface was used to detect the pressure jump from the shock wave, which then served as a trigger to fire the lasers at predetermined delay times.

Planar laser-induced fluorescence (PLIF) was used to produce one pre-shock initial condition image and two post-shock images. For all three images, Lambda Physik excimer lasers (248 nm) were pulsed once (25-30 ns duration) with an energy of approximately 500 mJ, and Andor CCD (1024×1024 pixel array) cameras were used to record the fluorescence signal.

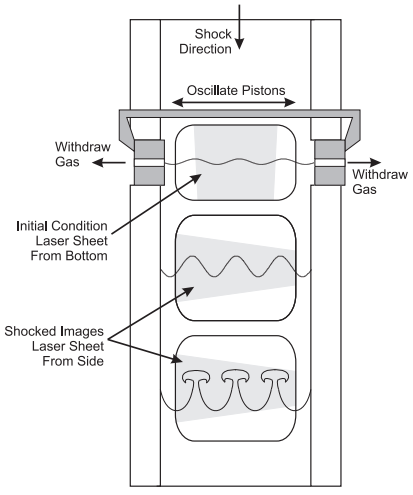

Fig. 1. Schematic of shock tube interface section with piston system, and imaging windows.

3 Computational Setup

Concurrently, hydrodynamic computations were performed using a 2-D hydrodynamics code (RAPTOR) that solves the multi-fluid compressible Euler equations, with an ideal gas law equation of state. A shock-capturing scheme and higher-order Godunov solver was used to handle shock propagation accurately and suppress spurious oscillations [8]. The calculations utilized a fixed (Eulerian) grid in 2-D Cartesian geometry, 512 grid points in the transverse dimension, and two levels of adaptive mesh refinement (AMR) on the fluid interface. The experimental initial condition was characterized using a Fourier transform and then reconstructed for the computational initial condition. The interface was then smeared vertically using a hyperbolic tangent distribution fitted to the diffusion characteristics of the experimental interface. Calculations were carried out with two fluids: SF_6 below the interface, and a mixture of nitrogen and acetone vapor above the interface. The relative concentrations of nitrogen and acetone vapor, and the strength of the incident shock wave, corresponded to the values determined experimentally.

4 Initial Condition

A region of interest was extracted from the raw initial condition image, including either the entire width of the shock tube, or a single wavelength of the wave, Fig. 2. This image was first corrected for divergence with a conformal mapping algorithm that placed light rays in columns, and then for laser attenuation (due to acetone) by integrating Beer's Law along light rays. The image was then remapped to physical space, and a five pixel Gaussian blur was applied to each pixel, to reduce the levels of fine-scale noise in the image due to artifacts of the imaging technique. A Fourier transform was then performed on the interface determined by the 50% acetone concentration pixel locations (labeled Displacement, Fig. 3 to determine mode, amplitude, and phase content for use in the numerical simulations.

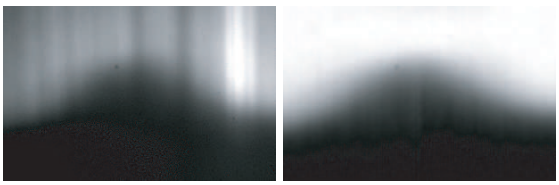

Fig. 2. Raw (left) and corrected (right) initial condition images.

The diffusion thickness was determined by finding the average vertical distance in which the acetone concentration increased from 10 to 90% of the maximum concentration. The average total diffusion thickness for the experiments was 2.38 cm, while the peak-to-peak amplitude of the initial condition for these experiments varied from 1.03 to 1.61 cm, Fig 3.

5 Results

For each experiment, the first post-shock image was taken approximately 2.8 ms after the shock initially contacted the interface, and the second image was taken at approx-

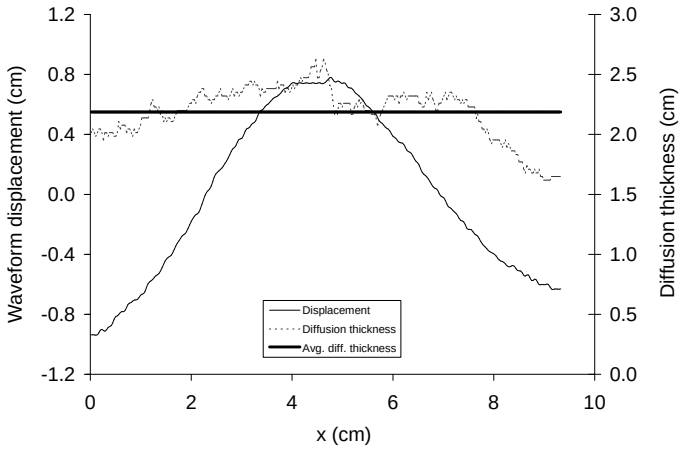

Fig. 3. Interface displacement and diffusion thickness along wavelength.

imately 5.3 ms. Figure 4 shows a progression in time for an experiment where the pistons were driven at 1.9 Hz for 3 revolutions. The initial condition images show that a predominantly single-mode (wavelength, λ=9.33 cm) waveform exists on the interface. Though the interface in the initial condition is notably diffuse, the passage of the shock wave results in a higher signal-to-noise ratio, as well as a gradient intensification due to shock-induced compression since the interface becomes much more visibly distinct in the post-shock images. For the portions of the initial waveform farthest from the walls, the typical Richtmyer-Meshkov growth can be observed over time. A bubble feature grows vertically into the lighter fluid, forms rollups, and develops the classic mushroom-like structure. Due to some higher mode content, the bubble is slightly asymmetric in the initial condition, giving the interface a larger slope on one side of the bubble than on the other. This results in greater baroclinic vorticity generation on the side with the larger slope. By using the initial condition obtained from the experiment as input, the simulation does an excellent job at reproducing the large length scale features of the instability development, however, there are fine-scale Kelvin-Helmholtz waves on the late time experimental image that do not appear in the simulation results.

The experimental results shown in Fig. 4, along with those from three additional cases, one at 1.9 and two 2.6 Hz, were analyzed to characterize the RM amplitude growth trends. Thus, four cases were considered: A and B at 2.6 Hz (λ=17.9 cm), and C and D and 1.9 Hz (λ=9.3 cm). A growth rate plot of non-dimensional length vs. non-dimensional time for one spike-bubble pair in each case was created using the initial condition analysis and measured post-shock interface amplitudes.

Following the analysis of Jones and Jacobs [6] and Jacobs and Krivets [9], the non-dimensional length was determined by taking ka-ka_0, where k is the wave number associated with the apparent wavelength of the initial condition waveform, a_0 is the initial amplitude, and a is the post-shock amplitude. The non-dimensional time was calculated as $k\dot{a}_0 t$, where $\dot{a}_0$ is the initial impulsive amplitude growth rate, and t is the time relative to shock arrival. A low-Mach number approximation [6] was used to find $\dot{a}_0$, using $\dot{a}_0 \approx ka_0 A\Delta V$, where A is the post shock Atwood number and ΔV is the shock wave velocity jump, both calculated from the measured shock strength using 1-D gasdynamics. The initial amplitude a_{0+} is the amplitude directly after the shock wave traverses the

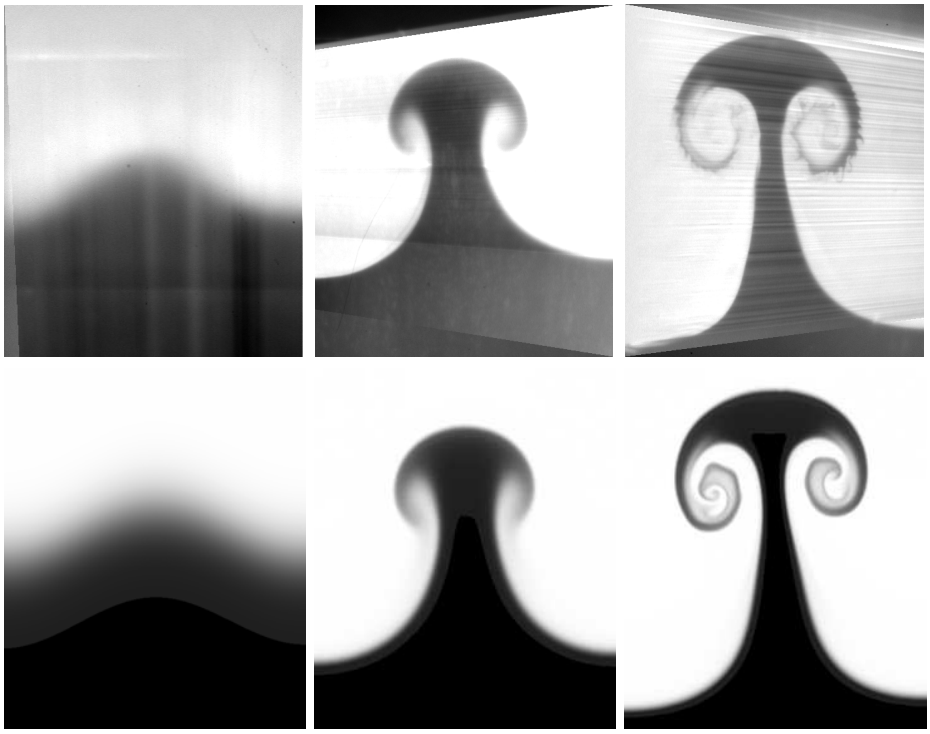

Fig. 4. Time-sequence of experimental images (top row) and computational images (bottom row) for a single wavelength from a piston driving frequency of 1.9 Hz, case D from Fig. 5.

interface. This amplitude takes into account compression and is derived by Meshkov's equation [3] $a_{0+} = a_0(1-V/c_1)$, where V is the post-shock interface velocity and c_1 is the shock speed in the light gas, both also calculated from 1-D gasdynamics. This analysis was applied to both the experimental data and to the results from the RAPTOR simulations outlined above. Figure 5 shows the resulting plot of non-dimensional amplitude vs. non-dimensional time for experimental and computational data.

6 Conclusions

The results shown in Fig. 5 indicate that substantial agreement exists between the RM growth trends found in both experiment and simulation, particularly for earlier times. At later times in the progression of the instability, the computational results appear to underestimate the full extent of the amplitude growth. The nondimensionalization technique appears to have been successful, though, as the two growth trends follow each other fairly closely. Overall, the experimental results show good agreement with the RAPTOR results.

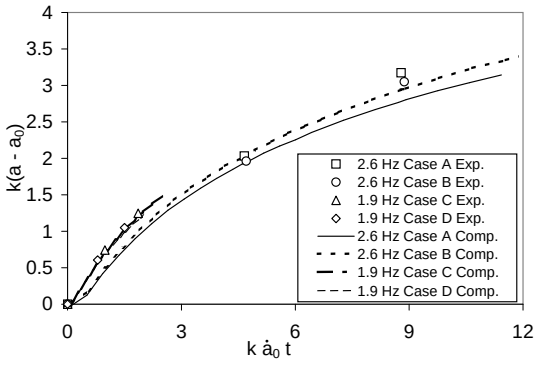

Fig. 5. Non-dimensional amplitude vs. non-dimensional time, measured experimentally and extracted from RAPTOR simulations, for a multimode sinusoid interface initially produced by piston oscillation at each of two different frequencies and accelerated by a M=1.3 shock wave.

Acknowledgement

The authors would like to acknowledge the financial support of the Department of Energy (through grant No. DE-FG52-03NA00061).

References

1. J.D. Kilkenny, et al: 'A review of the ablative stabilization of the Rayleigh-Taylor instability in regimes relevant to inertial confinement fusion,' Phys. Plasmas **1**(5) pp 1379–1389 (1994)
2. B. Jun, T.W. Jones, M.L. Norman: 'Interaction of Rayleigh-Taylor fingers and circumstellar cloudlets in young supernova remnants,' The Astrophysical Journal **468** pp L59–L63 (1996)
3. Ye.Ye. Meshkov: 'Instability of a shock wave accelerated interface between two gases.' NASA Technical Translation F-13,074 (1970)
4. J.G. Oakley: Experimental Study of Shocked Gas Interfaces with Visualized Initial Conditions. Ph.D. Thesis, University of Wisconsin-Madison (2001)
5. A. Bates, J.G. Oakley, M.H. Anderson, J. Greenough, R. Bonazza: 'Membraneless gas-gas initial condition for the Richtmyer-Meshkov instability,' *24th Intl. Symp. on Shock Waves Proc., Beijing China, Paper 2691* (2004)
6. M.A. Jones, J.W. Jacobs: 'A membraneless experiment for the study of Richtmyer-Meshkov instability of a shock-accelerated gas interface,' Phys. Fluids **9**(10) pp 3078–3085 (1997)
7. M.H. Anderson, B.P. Puranik, J.G. Oakley, P.W. Brooks, R. Bonazza: 'Shock tube investigation of hydrodynamic issues related to inertial confinement fusion,' Shock Waves **10**(5) pp 377–387 (2000)
8. P. Colella: 'A direct Eulerian MUSCL scheme for gas dynamics,' SIAM J. Sci. Stat. Comput. **6** pp 104 (1985)
9. J.W. Jacobs, V.V. Krivets: 'Experiments on the late-time development of single-mode Richtmyer-Meshkov instability,' Physics of Fluids **17** pp 034105–1:10 (2005)